Available online at www.sciencedirect.com
SCIENCE DIRECT®
Pergamon
Acta Materialia 51 (2003) 1789–1799
Acta MATERIALIA
www.actamat-journals.com

The morphology and crystallography of lath martensite in Fe-C alloys

S. Morito [a,*], H. Tanaka [b], R. Konishi [c 1], T. Furuhara [a], T. Maki [a]

[a] *Department of Materials Science and Engineering, Kyoto University, Yoshida-honnmachi, Sakyo-ku, Kyoto 606-8501, Japan*
[b] *Nippon Steel Co., 1-1 Tobihatacho, Tobihata-ku, Kitakyushu, Fukuoka 804-8501, Japan*
[c] *Graduate student, Kyoto University, Japan*

Received 18 October 2002; received in revised form 20 November 2002; accepted 30 November 2002

Abstract

The morphology and crystallography of lath martensite in Fe-C alloys containing various carbon contents from 0.0026 to 0.61% were studied by analyzing electron back scattered diffraction patterns in scanning electron microscopy and Kikuchi diffraction patterns in transmission electron microscopy. As carbon content increases, the sizes of both packet and block decrease. In low carbon steels (0.0026–0.38%C), a block which is observed as having different contrasts under optical microscopy contains two groups (sub-blocks) of laths which are of two K-S variants with a misorientation of about 10 degrees. On the other hand, in the high carbon alloy (0.61%C), a block consists of laths of a single K-S variant.

Keywords: lath martensite; iron-carbon alloy; morphology and crystallography; electron back scattered diffraction pattern; Kikuchi diffraction pattern

1. Introduction

Ferrous martensite exhibits a variety of morphologies [1], i.e. lath, butterfly, lenticular and thin-plate. Among them, lath martensite has overwhelming industrial significance because it appears in most heat-treatable commercial steels. The size of martensite lath is very small, and hence individual laths are not clearly observed in optical micrographs. However, since lath martensites have a tendency to align themselves parallel to one another in the large area of the parent grain, lath martensite exhibits a characteristic microstructure at the optical microscopic scale. Current views hold that an austenite grain is divided into packets (the group of laths with the same habit plane) and each packet is further subdivided into blocks (the group of laths of the same orientation (same variant))[2–4]. Since the strength and toughness of martensitic steels are strongly related to packet and block sizes (effective grain sizes in lath martensite structure) [5,6], the characteristics of morphology and crystallography of lath martensite are of great importance.

* Corresponding author. Tel.: +81-75-753-5475; fax: +81-75-753-4861.
E-mail address: morito@iron.mtl.kyoto-u.ac.jp (S. Morito).
[1] Nippon Steel Co., 1-1 Tobihatacho, Tobihata-ku, Kitakyushu, Fukuoka 804-8501, Japan.

1359-6454/03/$30.00
doi:10.1016/S1359-6454(02)00577-3

There have been many studies conducted on the morphology and crystallography of lath martensite in Fe-alloys [1–21]. However, the crystallographic feature of lath martensite structure has not been completely clarified yet because of discrepancy between various experimental results. For example, the inter-variant relationships between neighboring blocks in a given packet have been reported to be twin-related [5,7] or non-twin relationship [3,8–10]. It is also not clear whether a packet consists of laths with all possible six variants of Kurdjumov–Sachs (K–S) relationship [11] or only few specific variants among possible six ones [2–5]. These inconsistencies in the previous studies might be caused by the inaccurate orientation measurement which was analyzed by the selected area electron diffraction pattern.

Recently, however, new and more accurate techniques for the orientation measurement with a margin of error less than 1 degree, such as the Kikuchi diffraction pattern taken from local area on transmission electron microscopy (TEM), and the electron back scattered diffraction pattern (EBSP) on scanning electron microscopy (SEM), have been developed and used to study the crystallography of lath martensite. For example, Kelly et al. [12] reported, by the analysis of Kikuchi diffraction pattern obtained with a spot size of about 7nm, that the orientation between martensite and austenite in low carbon alloy steels is essentially the Greninger–Troiano relationship which is close to the K–S relationship with a deviation of a few degrees. Gourgues et al. [13] showed by EBSP measurement that martensite block boundaries in Fe-0.2C alloy are mainly not twin boundaries, but those with the misorientation of [011]/60 degrees. However, there has been no systematic study on the crystallography of lath martensite in Fe-C alloys with various carbon contents.

The purpose of the present study is to re-examine the morphology and crystallography of lath martensite in Fe-C alloys containing various carbon contents from 0 to 0.6 mass% by Kikuchi diffraction pattern and EBSP analyses.

2. Experimental procedure

An ultra-low carbon steel (interstitial free steel) with 0.0026 mass% C and 0.14 mass% Mn (hereafter Fe-0.0026C) and Fe-0.18, 0.38 and 0.61mass% C alloys were used. Details of chemical compositions of these alloys are shown in Table 1. All specimens were austenitized at 1373K or 1573K and quenched in water or iced brine to obtain full lath martensite structure. Prior austenite grain size in the Fe-0.0026C alloy was 670 μm, and in other alloys about 200μm.

Microstructures were observed by optical microscope, SEM (Hitachi S3100H) and TEM (Philips CM200). EBSP analysis was made with the TSL Orientation Imaging Microscopy system. Kikuchi patterns obtained by the convergent beam method were analyzed by software for orientation determination developed by Zaefferer [22]. It was difficult to obtain clear Kikuchi patterns of as-quenched martensite in Fe-0.38C and Fe-0.61C alloys due to high density of dislocations. Therefore, for these two alloys, annealing at 773K for 0.6 ks was undertaken for accurate analysis of crystallographic orientations.

Since austenite does not exist at room temperature after quenching in the present alloys, it was impossible to directly measure the orientation relationship between martensite lath and austenite. However, if the orientation relationship between martensite and austenite is fixed, the misorientation of each variant pair can be determined uniquely [23]. The orientation relationship of martensite lath with austenite shows deviation around K–S, Greninger–Troiano and Nishiyama relationships. However, orientation relationships of most laths could be characterized as near K-S orientation relationships in the present study.

In the case of K–S orientation, there are 24 variants as listed in Table 2. Laths in a given packet have the same plane parallel relationship between close-packed planes (e.g. V1 to V6). Thus, there are four crystallographically different packets in an austenite grain. In a packet, there are six variants with different direction parallel relationships on the same conjugate parallel close packed plane. Fig. 1 shows the orientation relationship between austenite and six K-S variants (V1 to V6) within a packet.

Table 1
Chemical compositions of the alloys used [mass%]

	C	Si	Mn	P	S	Fe	Others
Fe-0.0026C	0.0026	<0.01	0.14	0.008	0.005	bal.	Ti:0.046, B:0.0024, Al:0.015
Fe-0.18C	0.18	0.006	0.02	<0.001	0.004	bal.	
Fe-0.38C	0.38	0.006	0.01	<0.001	0.004	bal.	
Fe-0.61C	0.61	0.014	0.01	0.003	0.005	bal.	

Table 2
Twenty-four variants in K–S relationship

Variant	Plane parallel	Direction parallel									Rotation from Variant 1	
No.		[	γ			]//[	α'			]	Axis (indexed by martensite)	Angle [deg.]
V1		[	−1	0	1	]//[	−1	−1	1	]	—	—
V2		[	−1	0	1	]//[	−1	1	−1	]	[0.5774–0.57740.5774]	60.00
V3	(111)γ	[	0	1	−1	]//[	−1	−1	1	]	[0.0000–0.7071-0.7071]	60.00
V4	//(011)α'	[	0	1	−1	]//[	−1	1	-1	]	[0.00000.70710.7071]	10.53
V5		[	1	−1	0	]//[	−1	−1	1	]	[0.00000.70710.7071]	60.00
V6		[	1	−1	0	]//[	−1	1	−1	]	[0.0000–0.7071–0.7071]	49.47
V7		[	1	0	−1	]//[	−1	−1	1	]	[-0.5774–0.57740.5774]	49.47
V8		[	1	0	−1	]//[	−1	1	−1	]	[0.5774–0.57740.5774]	10.53
V9	(1-11)γ	[	−1	−1	0	]//[	−1	−1	1	]	[−0.18620.76660.6145]	50.51
V10	//(011)α'	[	−1	−1	0	]//[	−1	1	−1	]	[−0.4904–0.46250.7387]	50.51
V11		[	0	1	1	]//[	−1	−1	1	]	[0.3543–0.9329–0.0650]	14.88
V12		[	0	1	1	]//[	−1	1	−1	]	[0.3568–0.71360.6029]	57.21
V13		[	0	−1	1	]//[	−1	−1	1	]	[0.93290.35430.0650]	14.88
V14		[	0	-1	1	]//[	-1	1	-1	]	[-0.73870.4625-0.4904]	50.51
V15	(-111)γ	[	-1	0	-1	]//[	-1	-1	1	]	[-0.2461-0.6278-0.7384]	57.21
V16	//(011)α'	[	-1	0	-1	]//[	-1	1	-1	]	[0.65890.65890.3628]	20.61
V17		[	1	1	0	]//[	-1	-1	1	]	[-0.65890.3628-0.6589]	51.73
V18		[	1	1	0	]//[	-1	1	-1	]	[-0.3022-0.6255-0.7193]	47.11
V19		[	-1	1	0	]//[	-1	-1	1	]	[-0.61450.1862-0.7666]	50.51
V20		[	-1	1	0	]//[	-1	1	-1	]	[-0.3568-0.6029-0.7136]	57.21
V21	(11-1)γ	[	0	-1	-1	]//[	-1	-1	1	]	[0.95510.0000-0.2962]	20.61
V22	//(011)α'	[	0	-1	-1	]//[	-1	1	-1	]	[-0.71930.3022-0.6255]	47.11
V23		[	1	0	1	]//[	-1	-1	1	]	[-0.7384-0.24610.6278]	57.21
V24		[	1	0	1	]//[	-1	1	-1	]	[0.91210.41000.0000]	21.06

When V1 is taken as a reference, the orientation relationship between V1 and V2 is a twin relationship ([011]/70.5 degrees, $\Sigma 3$). The orientation relationship between V1 and V3 or V5 is [011]/60.0 degrees, and between V1 and V6 is [011]/49.5 degrees, deviate by misorientation of about 10 to 20 degrees from the exact twin relationship. On the other hand, the misorientation between V1 and V4 is a low angle of about 10 degrees.

Fig. 2 shows [001]α' standard stereographic projection of one of the K–S variants (V1) on which the [001]α' axes of 23 other variants (V2 to V24) are plotted. The K–S variant of observed martensite lath can be identified by comparing the experimentally measured martensite/martensite

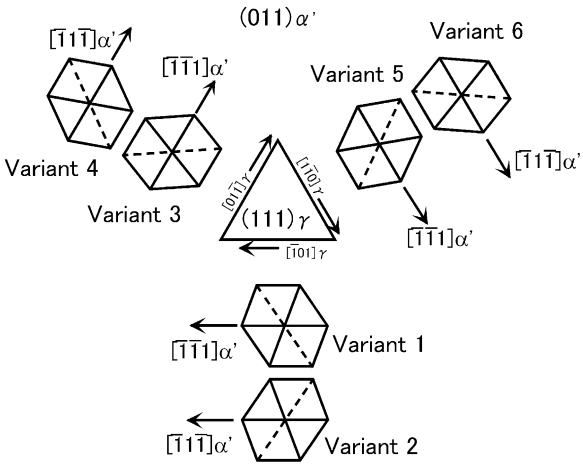

Variant	Misorientation from Variant 1 (V1)
V2	twin relation (Σ 3)
V3	10.53° from twin relation
V4	10.53°
V5	10.53° from twin relation
V6	21.06° from twin relation (Σ 11)

Fig. 1. Schematic illustration showing the orientations of K–S variants in a packet.

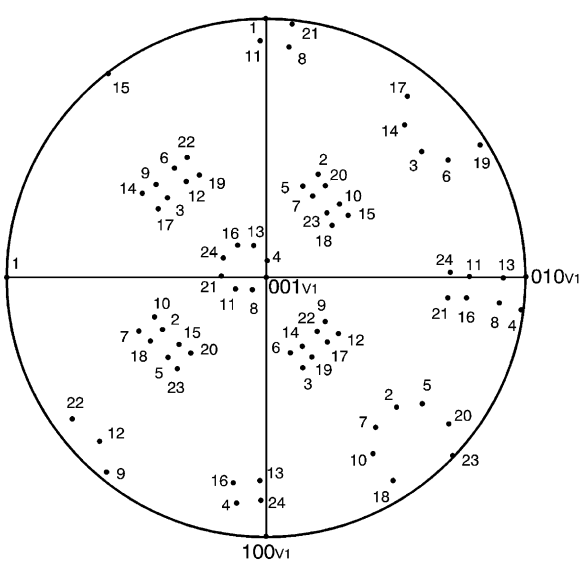

Fig. 2. [001]α′ standard stereographic projection of one of the K–S variants (V1) on which the [001]α′ axes of 23 other variants (V2 to V24) are plotted as solid marks.

orientation relationship with the calculated plot of Fig. 2. Actually, comparisons were made for 24 different calculated plots by taking each of the 24 variant as a reference.

3. Results

3.1. OM observation

Fig. 3 shows optical micrographs of lath martensite in Fe-C alloys with different carbon contents. In the Fe-0.0026C alloy (Fig. 3(a)), large parallel blocks are seen in a packet with strong contrast. The Fe-0.18C alloy, as shown in Fig. 3(b), also exhibits clear block structures, although they are slightly finer than the blocks in the Fe-0.0026C alloy. In the Fe-0.38C alloy (Fig. 3(c)), blocks and packets are finer than in the lower carbon alloys. Lath martensite in the Fe-0.61C alloy shows a rather uniform contrast, and it is difficult to recognize blocks and packets in the optical micrograph (Fig. 3(d)). These results are consistent with the previous results obtained by one of the present authors[21].

3.2. SEM and TEM observations

3.2.1. Fe-0.0026C alloy

Fig. 4(a) is an optical micrograph of a packet of 0.0026C lath martensite, and Figs. 4(b) and (c) are the corresponding crystal-orientation maps obtained by EBSP measurement. These colored maps show the orientations of laths for two directions of the specimen, i.e. normal and parallel to the polished surface, respectively. B1, B2 and B3 in Fig. 4(a) are different blocks within a packet. It is clear from Figs. 4(b) and (c) that the orientations of B1, B2 and B3 are entirely different to each other. It is to be noted that each block contains two different lath groups of about 5 μm width, misoriented by approximately 10 degrees (hereafter denoted as sub-blocks). The corresponding K–S variants were determined by EBSP analysis as shown in Figs. 4(b) and (c). Variants of sub-blocks in the blocks of B1, B2 and B3 are V2–V5, V1–V4 and V3–V6 with small misorientation, respectively.

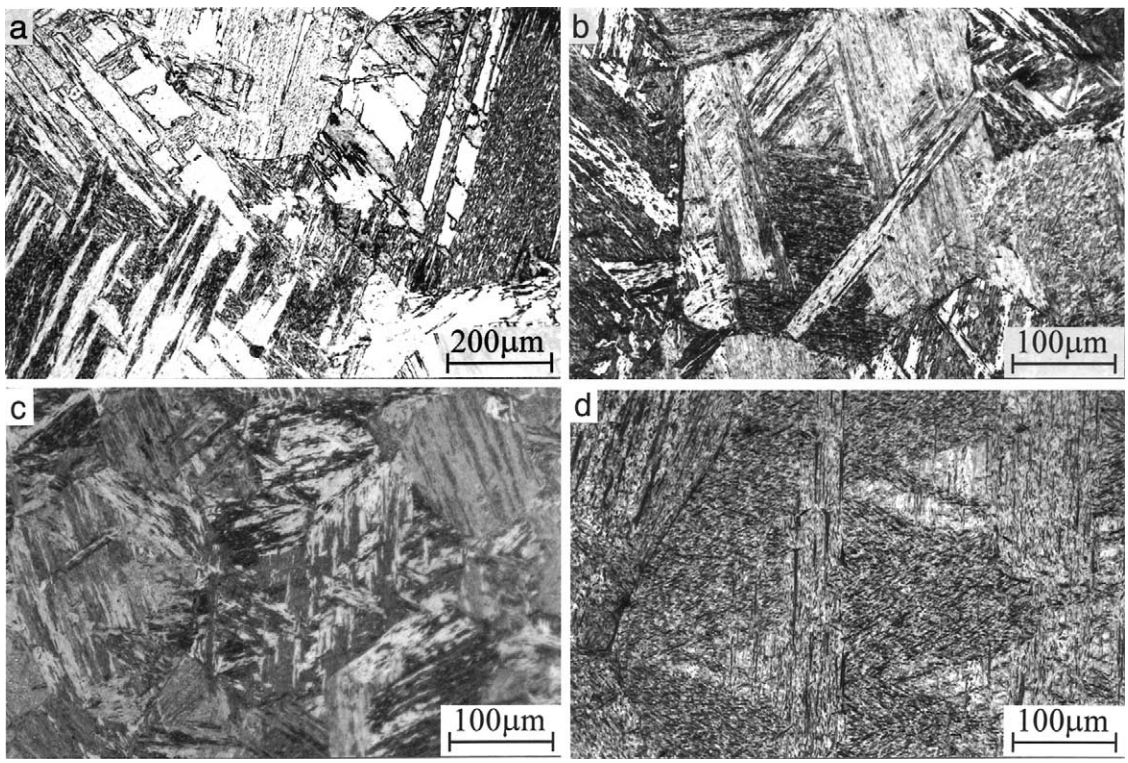

Fig. 3. Optical micrographs of lath martensite in (a) Fe-0.0026C, (b) Fe-0.18C, (c) Fe-0.38C and (d) Fe-0.61C alloys. Etching solution: 3% nital.

Fig. 5(a) shows the TEM image of lath martensite in a block. There observed two regions, 'a' and 'b' where the habit plane of laths are slightly different. Electron diffraction patterns taken from areas 'a' and 'b' indicate that these areas have slightly different crystallographic orientations. Fig. 5(b) shows the $<001>\alpha'$ poles measured by Kikuchi patterns of each lath in the areas 'a' and 'b'. It was confirmed that variants of laths in areas 'a' and 'b' are V1 and V4 respectively, which correspond to sub-blocks with a small misorientation in a single block in Fig. 4. Although orientation relationship of most of laths is close to the K–S relationship, laths with nearly Nishiyama orientation relationship are also observed as shown in Fig. 5(b). By the trace analysis, the habit plane of laths in the area 'a' was determined to be near (575)γ and the habit plane of laths in the area 'b' was (755)γ.

Fig. 6 is another example of crystal-orientation map of parallel blocks in a packet. Three blocks with different orientations are observed, and each block contains sub-blocks with a small misorientation. It appears from Figs. 4 and 6 that there is no specific rule for the orientation relationship between adjacent parallel blocks. Furthermore, a specific combination of two variants with a small misorientation, i.e. V1–V4, V2–V5 and V3–V6 makes a block, and then laths with all the six variants (V1 to V6) exist in a given packet. There are three types of combinations between adjacent blocks in a given packet, i.e. group 1: V1–V3, V3–V5, V5–V1, V2–V4, V4–V6 and V6–V2 (whose misorientation is [011]/60.0 degrees), group 2: V1–V6, V3–V2 and V5–V4 (whose misorientation is [011]/49.5 degrees) and group 3: V1–V2, V3–V4 and V5–V6 (whose misorientation is [111]/60.0 degree (= [011]/70.5 degrees)). Table 3 summarizes the observed results on the ratio of these variant combinations in various alloys. The observed ratio of group 1: group 2: group 3 in Fe-0.0026C alloy was about 2:1:1, which is identical to the

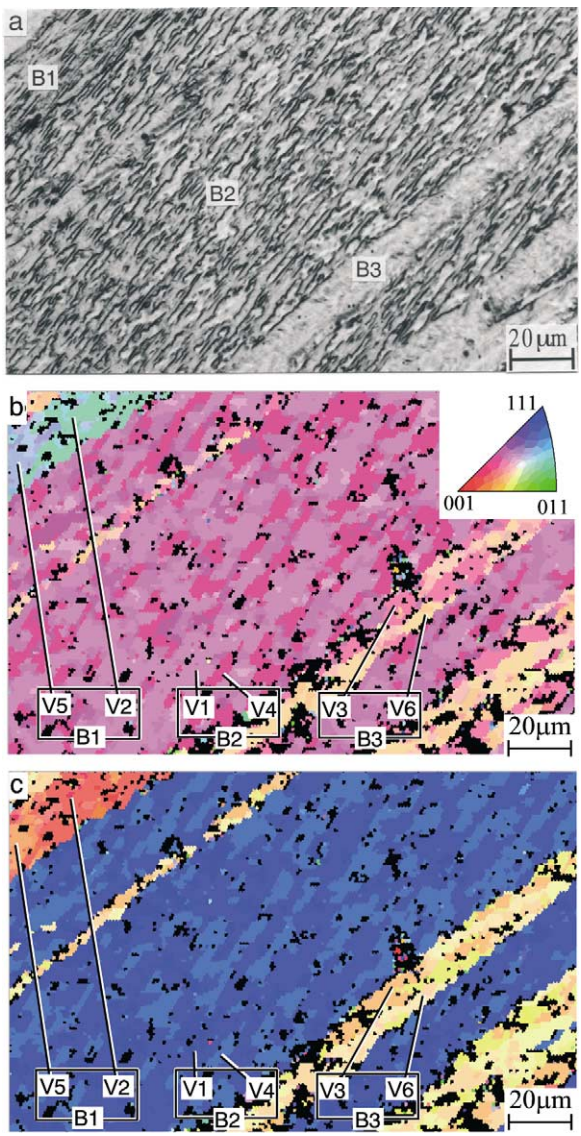

Fig. 4. (a) Optical micrograph of lath martensite in Fe-0.0026C alloy, and (b), (c) the corresponding crystal-orientation maps obtained by EBSP analysis for the directions of perpendicular and parallel to the polished surface, respectively.

same ratio of combinations between adjacent parallel blocks in which two variants (sub-blocks) are equal in fraction.

3.2.2. Low and high carbon alloys

Fig. 7(a) shows the SEM image of a packet of lath martensite in the Fe-0.18C alloy. The block

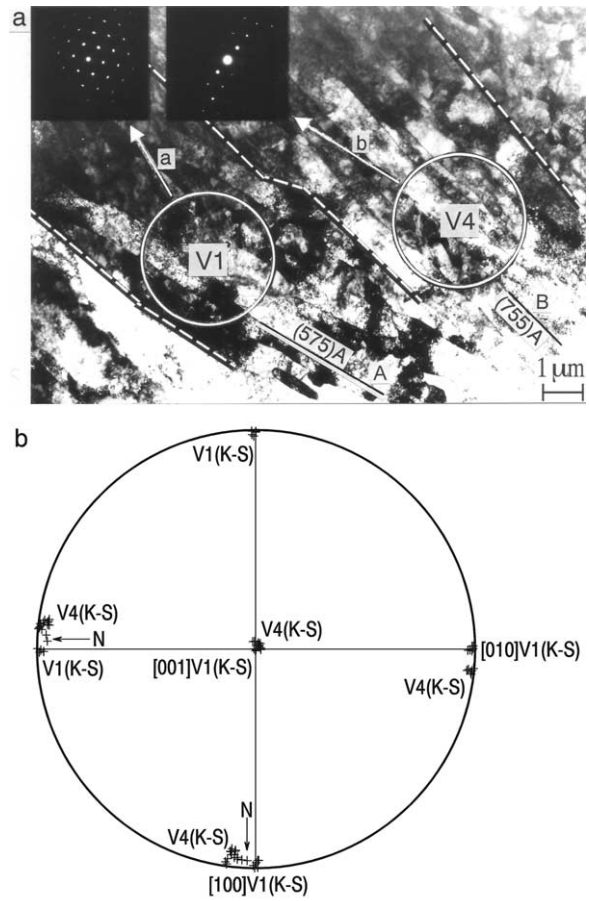

Fig. 5. (a) TEM image and electron diffraction patterns of lath martensite in Fe-0.0026C alloy and (b) the stereographic projection showing $<001>\alpha'$ poles (marked by '+') of each lath in Fig. 5 (a).

width of martensite seems narrower than that in the Fe-0.0026C alloy. The EBSP measurement (Fig. 7(b)) reveals that there are three parallel blocks with different orientations, and each block contains sub-blocks with low angle misorientation in the same way as the Fe-0.0026C alloy.

Figs. 8(a) and (b) show the SEM micrograph of a packet of 0.38C lath martensite and the corresponding crystal-orientation map, respectively. Blocks are finer and more degenerate in comparison with lath martensite of Fe-0.18C alloy. However, the presence of sub-blocks is still recognizable within a block. On the ratio of boundaries between blocks in a packet, group 1 boundaries

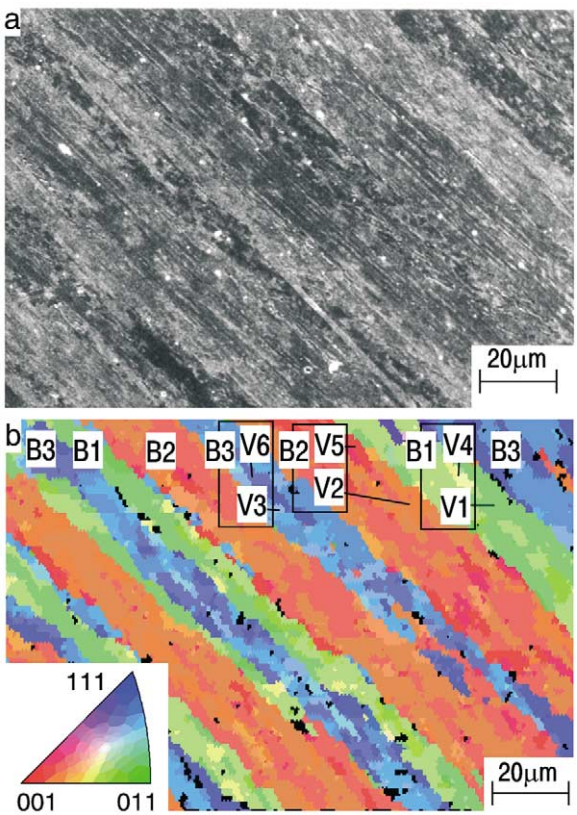

Fig. 6. (a) SEM image of lath martensite in Fe-0.0026C alloy and (b) the corresponding crystal-orientation map measured by EBSP.

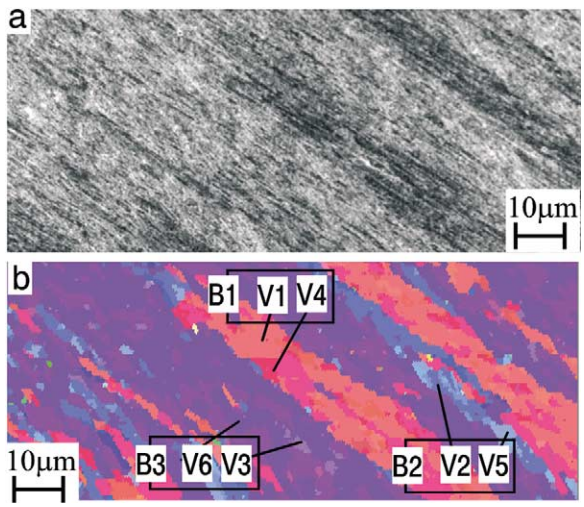

Fig. 7. (a) SEM image of lath martensite in Fe-0.18C alloy and (b) the corresponding crystal-orientation map measured by EBSP.

increase with increasing carbon content, as shown in Table 3.

Fig. 9(a) shows TEM microstructure of 0.61C lath martensite. The packets which consist of laths with the same habit plane exist and packet size is much smaller than in low carbon alloys. Fig. 9(b) shows the TEM microstructure of lath martensite in a packet in the Fe-0.61C alloy tempered at 773 K for 0.6 ks, and Fig. 9(c) is the corresponding variant map determined by Kikuchi pattern analysis. The block width in a packet is approximately equal to that of a few laths. It is clear that each block consists of laths with the same variant. Blocks of all the six variants (V1 to V6) are distributed randomly and there is no specific variant pair such as V1–V4, V2–V5 and V3–V6, which were observed as sub-blocks in the low carbon alloys.

Table 3
Observed ratio in three groups of block boundaries measured by EBSP analysis in various Fe-C alloys

Group	Rotation axis/angle	Corresponding variant pair	Ratio in block boundary area		
			Fe-0.0026C	Fe-0.18C	Fe-0.38C
1	[011]/60.0 deg.	V1–V3, V3–V5, V5–V1, V2–V4, V4–V6, V6–V2	56%	79%	83%
2	[011]/49.5 deg.	V1–V6, V3–V2, V5–V4	25%	7%	4%
3	[011]/70.5 deg.(Σ3) (=[111]/60.0 deg.)	V1–V2, V3–V4, V5–V6	19%	14%	12%

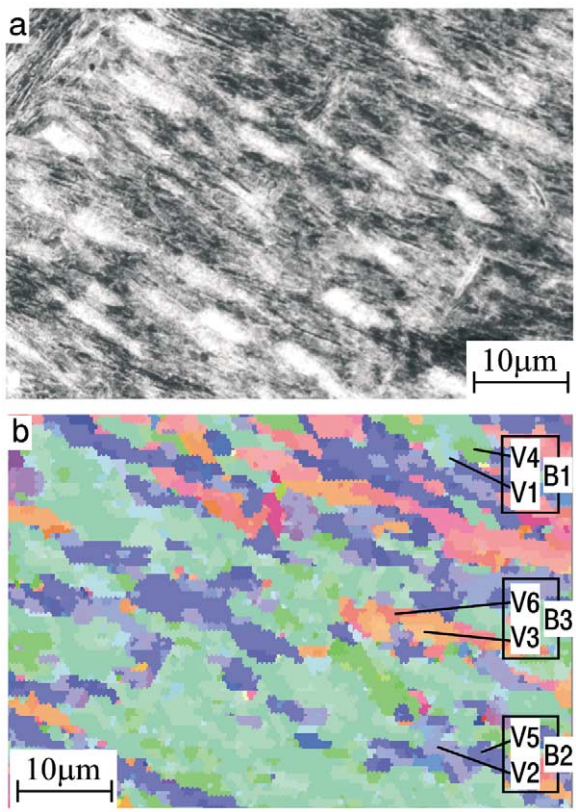

Fig. 8. (a) SEM image of lath martensite in Fe-0.38C alloy and (b) the corresponding crystal-orientation map measured by EBSP.

4. Discussion

In this study, the variation in the morphology and crystallography of lath martensite with carbon content was studied in detail. The present results are schematically summarized in Fig. 10. As carbon content increases from 0.0026% to 0.61%, block and packet sizes decrease. In low carbon alloys (0.0026%C–0.38%C, Fig. 10(a)), packets consist of well developed parallel blocks. There are three blocks with different orientations in a packet. Each block consists of laths of two specific K–S variant groups (sub-block) which are misoriented by small angles of about 10 degrees. In high carbon alloy (0.61%C, Fig. 10(b)), packets consist of fine blocks whose width is a few μm. Blocks consist of laths with a single variant and six blocks with different orientations exist in a packet.

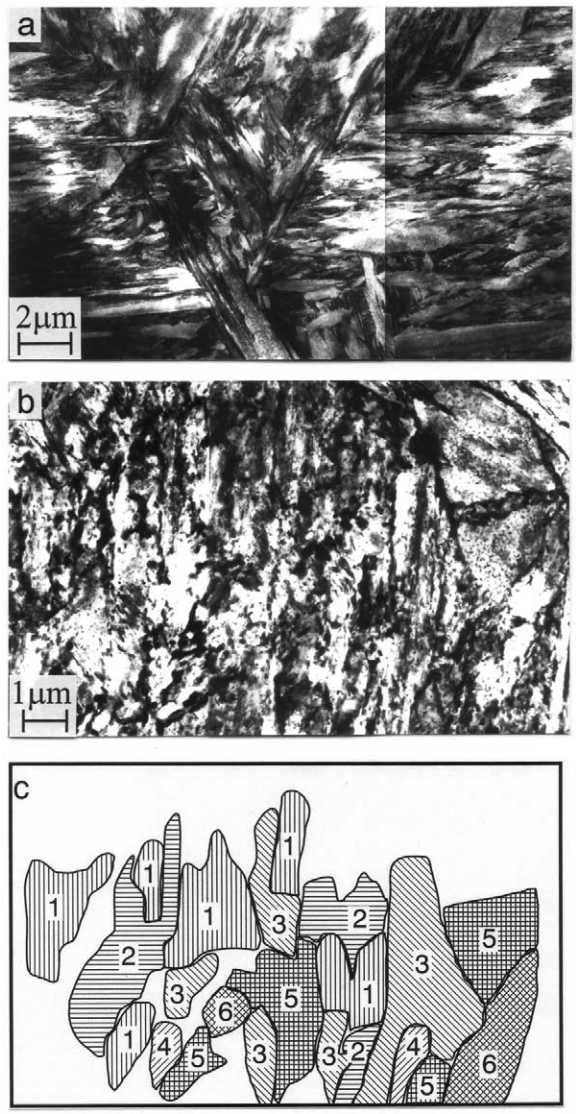

Fig. 9. TEM images of (a) quenched martensite and (b) tempered martensite in a packet in Fe-0.61C alloy and (c) the corresponding variant map of (b). Numbers in (c) indicate the number of K–S variants.

In the case of lenticular or thin plate martensite, it is known that adjacent martensite plates usually have the specific combination of variants in order to accommodate the transformation strain [24,25]. However, in the case of lath martensite, the accommodation of transformation strain by the combination of variants has not been clear yet. Thus, in the present study, the strains for the combinations

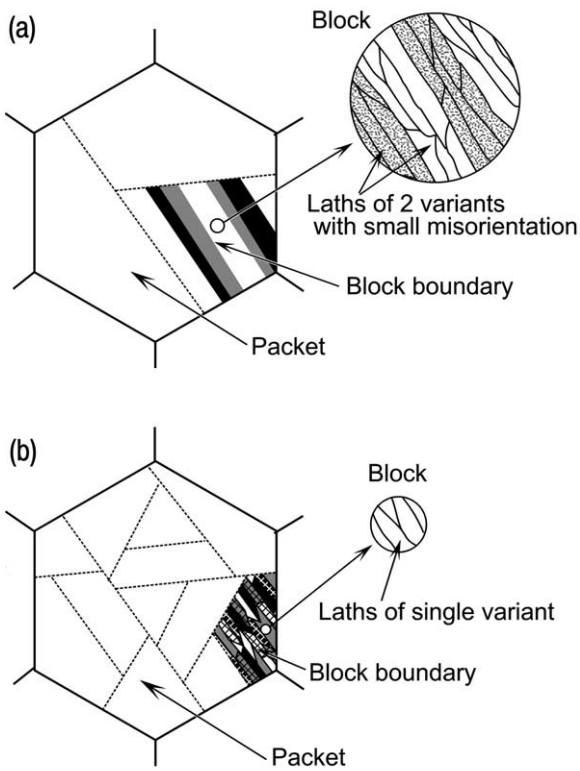

Fig. 10. Schematic illustrations showing lath martensite structure in (a) low carbon (0–0.4%C) and (b) high carbon (0.6%C) alloys.

of V1 with the other variants (V2 to V6) in a given packet of lath martensite were calculated as follows. The phenomenological theory of martensite crystallography developed by Kelly [26,27] with double lattice invariant shears [28] was used to calculate the shape strain for each martensite variant. For the analysis in Fe-0.0026C alloy, lattice parameters of austenite and ferrite [29], and Ms temperature [30] of pure iron were used. The lattice parameters at Ms temperature, 993K in pure iron were calculated with the experimentally obtained thermal expansion coefficient [31].

The calculated results are summarized in Table 4. The shape strain matrix F in the original phenomenological theory is given as:

$$F = RBS_2S_1 \quad (1)$$

where S_1 and S_2 are the first and second lattice invariant shears, and B and R correspond to Bain distortion and a rigid body rotation matrix, respectively. The selections of S_1 and S_2 are the same in the analysis made by Kelly[27]. Table 5 shows the habit plane and shape strain direction of lath of each variant (V1 to V6) in a given packet. Table 6 shows the total strains for the combinations of V1 with the other variants in a packet. The shape strain of the V1–V6 pair is the smallest. The combination of V1–V2 (Σ3 combination) does not cancel the shear strain effectively. Further, the shape

Table 4
Results of calculation for pure iron

Input		
Lattice parameter:	at Ms (993K) temperature	
Austenite:	a_0 = 0.36313 nm	
Martensite:	a = 0.28974 nm	
Lattice invariant shear		
S_1:	(101)[−101]γ	(112)[−1–11]α′
S_2:	(100)[01–1]γ	(110)[−11–1]α′
Shape strain of S_2:	0.09122	
Output		
Shape strain of S_1	0.26488	
Habit plane:	(0.49714, 0.71113, 0.49714)γ	
Shape strain direction:	[−0.20113, 0.70712, −0.67789]γ	
Shape strain matrix (F):	$\begin{pmatrix} 0.97578 & -0.03465 & -0.02422 \\ 0.08515 & 1.12181 & 0.08515 \\ -0.08164 & -0.11677 & 0.91837 \end{pmatrix}$	
Shape strain of F:	0.24223	
Orientation relationship:	(111)A - (011)α′:	0.23 degree
	[-101]A - [-1-11]α′:	3.41 degree

Table 5
Habit plane and shape strain direction of each variant in a packet in pure iron

Variant No.	Habit plane	Shape strain direction
V1	(5,7,5)γ	[−0.20,0.71,−0.68]γ
V2	(5,7,5)γ	[—0.68,0.71,−0.20]γ
V3	(7,5,5)γ	[0.71,−0.68,−0.20]γ
V4	(7,5,5)γ	[0.71,−0.20,−0.68]γ
V5	(5,5,7)γ	[−0.68,−0.20,0.71]γ
V6	(5,5,7)γ	[−0.20,−0.68,0.71]γ

strain of the combination of V1 and V4 which corresponds to a 'sub-block' in a block, is not so small compared with the other variant pairs. Therefore, the specific combination of V1–V4 in the block can not be explained by a self-accommodation calculated with the phenomenological theory developed by Kelly[27]. The origin of sub-blocks in a block in low carbon alloy is still unclear at present.

From the present study, it became clear that block and packet sizes decrease as carbon content increases. Furthermore, in the high carbon alloy, each block consists of laths with the same variant and blocks of all the six variants in a packet are distributed randomly. One possible reason why blocks and packets become finer can be the following. In low carbon alloys, laths in a large block are formed by autocatalysis and significant plastic accommodation might occur in the austenite matrix. However, in high carbon alloys, the strain of martensitic transformation could not be easily relieved by plastic accommodation in austenite matrix, because the austenite is harder than in low carbon alloys due to solid solution hardening by carbon, lower Ms temperatures, etc. For this reason, self-accommodation by the combination of martensite laths should take place more extensively. For self-accommodation, it is necessary that blocks and packets size decreases and all variants in a packet appear, resulting in the formation of blocks and packets with small size and random distribution of variants.

5. Conclusions

The morphology and crystallography of lath martensite in Fe-C alloys with different carbon contents such as 0.0026, 0.18, 0.38 and 0.61 mass% were examined by means of OM, SEM and TEM. Main results obtained are as follows:

1. As carbon content increases from 0.0026% to 0.61%, block and packet sizes decrease.
2. The orientation relationship between austenite and martensite is near Kurdjumov-Sachs relationship and some laths seem to have nearly Nishiyama relationship.
3. In low carbon alloys (0.0026%C–0.38%C), packets consist of well developed parallel blocks. There are three blocks with different orientations in a packet. Each block consists of laths of two specific K–S variant groups (sub-block) which are misoriented by small angles of about 10 degrees.
4. In high carbon alloy (0.61%C), packets consist of fine blocks whose width is a few μm. Blocks consist of laths with a single variant and six blocks with different orientations exist in a packet.

Acknowledgements

The authors wish to thank Dr. S. Zaefferer at the Max Planck Institute for Iron Research (Düsseldorf, Germany) for allowing us to use the program for on/off-line crystallographic analysis on TEM. The financial supports of the Iron and Steel Institute of Japan and the Ministry of Edu-

Table 6
Total shape strain in variant combinations in a packet

Combination of variants	V1	V1+V2	V1+V3	V1+V4	V1+V5	V1+V6	All 6 variants
Shape strain	0.242	0.228	0.123	0.186	0.123	0.049	0.024

cation, Science and Culture through a Grand-in-Aid for Encouragement of Young Scientists (B) No.14750575 are gratefully acknowledged.

References

[1] Maki T. Mater. Sci. Forum 1990;56-8:157.
[2] Matsuda S, Inoue T, Mimura H, Okamura Y. In: Proc. of Int. Sympo. on Toward Improved Ductility and Toughness. Kyoto, Japan, 1971:47.
[3] Marder AR, Krauss G. Trans. ASM 1967;60:651.
[4] Marder JM, Marder AR. Trans. ASM 1969;62:1.
[5] Inoue T, Matsuda S, Okamura Y, Aoki K. Trans. JIM 1970;11:36.
[6] Swarr T, Krauss G. Metall. Trans. A 1976;7A:41.
[7] Kelly PM. Acta Metall 1965;13:635.
[8] Wakasa K, Wayman CM, Kubo H, Shimizu K. Scripta Metall 1980;14:261.
[9] Wakasa K, Wayman CM. Metallography 1981;14:49.
[10] Apple CA, Caron RN, Krauss G. Metall. Trans 1974;5:593.
[11] Schastlivtsev VM, Blind LB, Rodionov DP, Yakovleva IL. Phys. Met. Metall 1988;66:123.
[12] Kelly PM, Jostsons A, Blake RG. Acta Metall. Mater 1990;38:1075.
[13] Gourgues AF, Flower HM, Lindley TC. Mater. Sci. and Technol 2000;16:26.
[14] Sarikaya M, Tokushige H, Thomas G. In: Proc. of Int. Conf. on Martensitic Transformations. Nara, Japan, 1986:613.
[15] Marder AR, Krauss G. Trans. ASM 1969;62:957.
[16] Chilton JM, Barton CJ, Speich GR. J. Iron Steel Inst 1970;208:184.
[17] Schoen FJ, Nilles JL, Owen WS. Metall. Trans 1971;2:2489.
[18] Law NC, Howell PR, Edmonds DV. Met. Sci 1979;13:507.
[19] Rao BVN. Metall. Trans. A 1979;10:645.
[20] Van Gent A, Van Doorn FC, Mittemeijer EJ. Metall. Trans. A 1985;16:1371.
[21] Maki T, Tsuzaki K, Tamura I. Trans. ISIJ 1980;20:207.
[22] Zaefferer S. J. Appl. Cryst 2000;33:10.
[23] Morito S, Tanaka H, Furuhara T, Maki T. In: Sakai T, Suzuki HG, editors. Proc. 4th Int. Conf. on Recrystallization and Related Phenomena. Sendai (JPN): Japan Institute of Metals, 1999: 295.
[24] Okamoto H, Oka M, Tamura I. Trans. JIM 1978;19:674.
[25] Bokros JC, Parker ER. Acta Metall 1963;11:1291.
[26] Wechsler MS, Lieberman DS, Read TA. Trans. AIME 1953;197:1503.
[27] Kelly PM. Mater. Trans. JIM 1992;33:235.
[28] Ross NDH, Crocker AG. Acta Metall 1970;18:405.
[29] Straumanis ME, Kim DC. Z. Metallk 1969;60:272.
[30] Nishiyama Z. Martensitic transformation. In: Fine ME, Meshii M, Wayman CM, editors. Transformation Temperature and Rate of Martensitic Transformation. New York: Academic Press; 1978. p. 224.
[31] Touloukian YS, Kirby RK, Taylor RE, Desai PD, editors. Thermal Expansion-Metallic Elements and Alloys. New York: IFI/Plenum; 1975. 157.